Published for SISSA by Springer

Received: *February 18, 2015*
Accepted: *April 7, 2015*
Published: *May 11, 2015*

A second Higgs from the Higgs portal

Adam Falkowski,[a] **Christian Gross**[b] **and Oleg Lebedev**[b]

[a] *Laboratoire de Physique Théorique, CNRS – UMR 8627, Université de Paris-Sud 11, F-91405 Orsay Cedex, France*
[b] *Department of Physics and Helsinki Institute of Physics, Gustaf Hällströmin katu 2, FI-00014 Helsinki, Finland*

E-mail: afalkows017@gmail.com, christian.gross@helsinki.fi, oleg.lebedev@helsinki.fi

Abstract: In the Higgs portal framework, the Higgs field generally mixes with the Standard Model (SM) singlet leading to the existence of two states, one of which is identified with the 125 GeV scalar observed at the LHC. In this work, we analyse direct and indirect constraints on the second mass eigenstate and the corresponding mixing angle. The existence of the additional scalar can be beneficial as it can stabilise the otherwise-metastable electroweak vacuum. We find parameter regions where all of the bounds, including the stability constraints, are satisfied. We also study prospects for observing the decay of the heavier state into a pair of the 125 GeV Higgs-like scalars.

Keywords: Higgs Physics, Beyond Standard Model

ArXiv ePrint: 1502.01361

doi:10.1007/JHEP05(2015)057

JHEP05(2015)057

Contents

JHEP05(2015)057

1 Introduction

The Higgs sector of the SM has a special feature that it can couple at the renormalisable level to the hidden sector [1–8]. In particular, the Higgs bilinear $H^\dagger H$ is the only dimension-2 operator of the SM that is gauge and Lorentz invariant. This allows for an interaction term

$$\Delta V = \frac{\lambda_{hs}}{2} H^\dagger H \, s^2 \,, \tag{1.1}$$

where s is a real SM-singlet scalar. Given that s develops a vacuum expectation value, the Higgs boson mixes with the singlet leading to the existence of two mass eigenstates $H_{1,2}$. In this work, we explore constraints on this scenario from various direct LEP and LHC searches, electroweak data and the Higgs couplings data.

Further motivation for exploring this model comes from stability issues of the SM. The current Higgs and top quark data favour metastability of the electroweak vacuum [9–11]. Although the existence of a deep global minimum in the scalar potential may not be problematic for current particle physics, it does raise some questions about early Universe physics, in particular, the inflationary stage [12]. These issues are avoided altogether if the Higgs potential receives a correction due to new physics which makes it convex at large field values. The simplest option is to couple the Higgs to a real scalar, in which case even a tiny mixing between the two can lead to a stable potential [13, 14]. Here we explore this mechanism for a more general mixing angle and study how large it is allowed to be by the current data. Some work in this direction has already been done in ref. [15–17], while

experimental constraints on the singlet portal have also been recently discussed in ref. [18–20]. We update and extend these studies. We explore the full range of the singlet-like scalar masses, including the region where it is lighter than 125 GeV. We take into account the most up-to date constraints from coupling measurements of the 125 GeV Higgs boson, and from searches for an additional Higgs-like scalar at the LHC and other experiments. We also perform a comprehensive analysis of constraints on the Higgs portal scenario from electroweak precision tests.

An interesting signature of the Higgs portal is the decay of the heavier state H_2 into a pair of the Higgs-like states H_1 [21, 22], whenever it is allowed kinematically. We find, in fact, that it is allowed in most of the parameter space favoured by the stability considerations. The relevant cross section for this process is at the picobarn level for a light H_2, which makes it observable at the LHC run-II (see also ref. [23]).

In the next section, we review the structure of the scalar potential. We then proceed to analysing the stability conditions, the experimental constraints and finally implications for the LHC new physics searches.

2 The model

We consider an extension of the SM by a real scalar gauge-singlet field s, which couples to the SM Higgs field via the potential

$$V(h,s) = \frac{\lambda_h}{4}h^4 + \frac{\lambda_{hs}}{4}h^2 s^2 + \frac{\lambda_s}{4}s^4 + \frac{1}{2}\,\mu_h^2\,h^2 + \frac{1}{2}\mu_s^2\,s^2\,. \tag{2.1}$$

Here, $(0, h/\sqrt{2})$ denotes the SM Higgs doublet in the unitary gauge. By construction, the above potential has the Z_2 symmetry $s \to -s$. This could also be thought of as a remnant of a U(1) symmetry in the hidden sector, under which a complex scalar field S transforms and whose imaginary part is gauged away.

In order to produce realistic W and Z boson masses, h must attain a VEV $\langle h\rangle \simeq 246.2$ GeV. In this paper, we consider the situation where also s has a non-zero VEV.[1] For both h and s non-vanishing, the potential is stationary at

$$\langle h\rangle^2 = \frac{2\lambda_{hs}\mu_s^2 - 4\lambda_s\mu_h^2}{4\lambda_h\lambda_s - \lambda_{hs}^2} \equiv v^2\,, \qquad \langle s\rangle^2 = \frac{2\lambda_{hs}\mu_h^2 - 4\lambda_h\mu_s^2}{4\lambda_h\lambda_s - \lambda_{hs}^2} \equiv w^2\,. \tag{2.2}$$

The mass matrix at this point is

$$\mathcal{M}^2 = \begin{pmatrix} 2\lambda_h v^2 & \lambda_{hs} v w \\ \lambda_{hs} v w & 2\lambda_s w^2 \end{pmatrix}\,. \tag{2.3}$$

Since the couplings are real and we require $v^2 > 0, w^2 > 0$, the mass matrix $\mathcal{M}^2$ is positive definite if and only if

$$\lambda_h > \frac{\lambda_{hs}^2}{4\lambda_s}\ , \quad \lambda_s > 0\ . \tag{2.4}$$

[1] The associated domain wall problem can be avoided either by a adding a tiny s^3 term to the Lagrangian or by treating our model as a low energy limit of a gauge theory (see above).

JHEP05(2015)057

$\mathcal{M}^2$ can be diagonalised by the orthogonal transformation $O^T\mathcal{M}^2O = \mathrm{diag}(m^2_{H_1}, m^2_{H_2})$, where

$$O = \begin{pmatrix} \cos\theta & \sin\theta \\ -\sin\theta & \cos\theta \end{pmatrix} \tag{2.5}$$

and the angle θ satisfies

$$\tan 2\theta = \frac{\lambda_{hs} v w}{\lambda_s w^2 - \lambda_h v^2} \,. \tag{2.6}$$

The mass squared eigenvalues are given by

$$m^2_{H_{1,2}} = \lambda_h v^2 + \lambda_s w^2 \mp \frac{\lambda_s w^2 - \lambda_h v^2}{\cos 2\theta} \,. \tag{2.7}$$

Note that we are using a different convention for θ compared to that of [13, 24]. The above equation implies $\mathrm{sign}(m^2_{H_2} - m^2_{H_1}) = \mathrm{sign}(\cos 2\theta)\,\mathrm{sign}(\lambda_s w^2 - \lambda_h v^2)$. The fields in the mass eigenstate basis are

$$\begin{pmatrix} H_1 \\ H_2 \end{pmatrix} = \begin{pmatrix} \cos\theta\,(h - \langle h\rangle) - \sin\theta\,(s - \langle s\rangle) \\ \cos\theta\,(s - \langle s\rangle) + \sin\theta\,(h - \langle h\rangle) \end{pmatrix} \,. \tag{2.8}$$

In the following, H_1 is always identified with the 125 GeV boson discovered at the LHC.

As we are interested in stability properties of the vacuum, it is useful to point out that our Z_2-symmetric potential subject to (2.4) has a *single* local minimum at tree level (barring the reflected minimum $w \to -w$). Indeed, as detailed in [24], the stationary points are local minima under the following conditions:

$$\begin{aligned}
&v \neq 0, w \neq 0 \;:\; \lambda_{hs}\mu_s^2 - 2\lambda_s\mu_h^2 > 0\,,\; \lambda_{hs}\mu_h^2 - 2\lambda_h\mu_s^2 > 0\,,\\
&v \neq 0, w = 0 \;:\; \lambda_{hs}\mu_h^2 - 2\lambda_h\mu_s^2 < 0\,,\; \mu_h^2 < 0\,,\\
&v = 0, w \neq 0 \;:\; \lambda_{hs}\mu_s^2 - 2\lambda_s\mu_h^2 < 0\,,\; \mu_s^2 < 0\,,\\
&v = 0, w = 0 \;:\; \mu_h^2 > 0\,,\; \mu_s^2 > 0\,.
\end{aligned} \tag{2.9}$$

These conditions are not compatible with each other and only one of them can correspond to a local minimum. As long as radiative corrections are small, e.g. when there are no large logs, this situation persists at the loop level. However, at large field values additional minima may develop.

We will consider the possibility that the SM extended by the singlet is valid up to the Planck scale. This entails constraints on the couplings λ_i as those must remain perturbative and lead to a stable scalar potential. We will require absolute stability of the electroweak vacuum. Although metastability is sufficient for many applications, reconciling the existence of a deeper minimum with cosmology may be non-trivial. For that reason, we choose to impose the stronger condition.

Electroweak scale constraints are formulated more easily in terms of the parameters $(m^2_{H_1}, m^2_{H_2}, \sin\theta, v, \lambda_{hs})$. On the other hand, perturbativity and stability analyses favour

JHEP05(2015)057

the set $(\lambda_h, \lambda_s, \lambda_{hs}, v, w)$. The quartic couplings can be expressed in terms of the "more physical" parameters as

$$\lambda_h = \frac{m_{H_1}^2}{2v^2} + \sin^2\theta\ \frac{m_{H_2}^2 - m_{H_1}^2}{2v^2} \tag{2.10a}$$

$$\lambda_s = \frac{2\,\lambda_{hs}^2}{\sin^2 2\theta}\frac{v^2}{m_{H_2}^2 - m_{H_1}^2}\left(\frac{m_{H_2}^2}{m_{H_2}^2 - m_{H_1}^2} - \sin^2\theta\right)\,. \tag{2.10b}$$

We leave λ_{hs} as an independent variable as it is directly related to the decay rate of H_2 into a pair of H_1's, when the process is allowed kinematically.

Let us now write down the couplings of the scalars to the SM matter. Those involving a single scalar are given by

$$\mathcal{L} \supset \frac{H_1\cos\theta + H_2\sin\theta}{v}\left[2m_W^2 W_\mu^+ W^{\mu-} + m_Z^2 Z_\mu Z^\mu - \sum_f m_f \bar{f} f\right]\,. \tag{2.11}$$

Thus, the partial decay widths of H_1 into SM matter are universally suppressed with respect to those of the SM Higgs by $\cos^2\theta$. Similarly, the partial decay widths of H_2 into SM matter are those of a would-be SM Higgs with mass m_{H_2} universally suppressed by $\sin^2\theta$.

On top of that H_2 decays to H_1 pairs are possible if $m_{H_2} > 2m_{H_1} \sim 250\,\text{GeV}$, and H_1 decays into H_2 pairs are possible for $m_{H_2} < m_{H_1}/2 \sim 62.5\,\text{GeV}$. These decays are mediated by the scalar self-interaction terms which we parametrise as

$$\mathcal{L} \supset -\frac{\kappa_{112}}{2} v\sin\theta\ H_1^2 H_2 - \frac{\kappa_{221}}{2} v\cos\theta\ H_2^2 H_1\,, \tag{2.12}$$

where the couplings are given by

$$\kappa_{112} = \frac{2m_{H_1}^2 + m_{H_2}^2}{v^2}\left(\cos^2\theta + \frac{\lambda_{hs}v^2}{m_{H_2}^2 - m_{H_1}^2}\right)\,, \tag{2.13a}$$

$$\kappa_{221} = \frac{2m_{H_2}^2 + m_{H_1}^2}{v^2}\left(\sin^2\theta + \frac{\lambda_{hs}v^2}{m_{H_1}^2 - m_{H_2}^2}\right)\,. \tag{2.13b}$$

In the kinematically allowed regime the decay widths are given by

$$\Gamma(H_2 \to H_1 H_1) = \frac{\sin^2\theta\ \kappa_{112}^2 v^2}{32\pi\, m_{H_2}}\sqrt{1 - \frac{4m_{H_1}^2}{m_{H_2}^2}}\,, \tag{2.14a}$$

$$\Gamma(H_1 \to H_2 H_2) = \frac{\cos^2\theta\ \kappa_{122}^2 v^2}{32\pi\, m_{H_1}}\sqrt{1 - \frac{4m_{H_2}^2}{m_{H_1}^2}}\,. \tag{2.14b}$$

3 Vacuum stability and perturbativity

Here we study what constraints are imposed on the parameter space if we require the couplings to remain perturbative and the electroweak vacuum to be stable all the way up to the Planck scale (see also [25, 26]).

JHEP05(2015)057

The potential has 5 parameters of which 2 are fixed by requiring $v = 246.2$ GeV and $m_{H_1} = 125.15$ GeV. As the remaining 3 parameters we choose the mass m_{H_2} of the heavier state H_2, the admixture $\sin\theta$ of the singlet to the state H_1 and the coupling λ_{hs}. For given values of $m_{H_2}, \sin\theta$ and λ_{hs}, the corresponding values of λ_h and λ_s are determined by eqs. (2.10a), (2.10b). The resulting couplings λ_h, λ_s and λ_{hs} are evolved to the Planck scale $m_P = 2.4 \times 10^{18}$ GeV using one-loop RG evolution. The relevant RGEs (neglecting all the Yukawa couplings except for y_t) read

$$\begin{aligned}
16\pi^2 \frac{d\lambda_h}{dt} &= 24\lambda_h^2 - 6y_t^4 + \frac{3}{8}\left(2g^4 + (g^2+g'^2)^2\right) + (-9g^2 - 3g'^2 + 12y_t^2)\lambda_h + \frac{1}{2}\lambda_{hs}^2 \,, \\
16\pi^2 \frac{d\lambda_{hs}}{dt} &= 4\lambda_{hs}^2 + 12\lambda_h\lambda_{hs} - \frac{3}{2}(3g^2 + g'^2)\lambda_{hs} + 6y_t^2\lambda_{hs} + 6\lambda_s\lambda_{hs} \,, \\
16\pi^2 \frac{d\lambda_s}{dt} &= 2\lambda_{hs}^2 + 18\lambda_s^2 \,, \\
16\pi^2 \frac{dy_t}{dt} &= y_t\left(\frac{9}{2}y_t^2 - \frac{17}{12}g'^2 - \frac{9}{4}g^2 - 8g_3^2\right) \,, \\
16\pi^2 \frac{dg_i}{dt} &= b_i\, g_i^3 \quad \text{with} \quad (b_1, b_2, b_3) = (41/6, -19/6, -7) \,,
\end{aligned} \tag{3.1}$$

where $g_i = (g', g, g_3)$ denotes the gauge couplings. As input values we use $g(m_t) = 0.64$, $g'(m_t) = 0.35$, $g_3(m_t) = 1.16$ and $y_t(m_t) = 0.93$. Our input top Yukawa coupling is based on the central value of $m_t(m_t)$ advocated in [27].

The vacuum stability conditions depend on the sign of λ_{hs} (cf. also the discussion in ref. [14]):

$\boldsymbol{\lambda_{hs} > 0}$. The requirement $\lambda_h > \lambda_{hs}^2/(4\lambda_s)$ has to be met only around the mass scale of the fields (i.e. around the TeV scale in our case) in order for v, w to be a minimum of the potential. It may not however hold at the high energy scale. As long as the quartic couplings are positive $\lambda_i > 0$, the potential is positive definite and no run-away direction exists.

$\boldsymbol{\lambda_{hs} < 0}$ Neglecting the quadratic terms, the potential can be written as

$$V \simeq \frac{1}{4}\left[\left(\sqrt{\lambda_h}\, h^2 - \sqrt{\lambda_s}\, s^2\right)^2 + \left(\lambda_{hs} + 2\sqrt{\lambda_h\lambda_s}\right) h^2 s^2\right] . \tag{3.2}$$

This shows that V has a run-away direction at large field values unless $\lambda_h > \lambda_{hs}^2/(4\lambda_s)$. This condition and $\lambda_s > 0$ are therefore to be imposed at all scales.

In figure 1, we show, for different weak scale values of λ_{hs}, the area in the $m_{H_2} - |\sin\theta|$ plane where $\lambda_h, \lambda_s, \lambda_{hs}$ remain perturbative ($\lambda_i < 4\pi^2$) up to m_P and where the electroweak vacuum remains stable.[2] Qualitatively, the shape of the allowed regions can be understood as follows:

[2]Note that imposing a stricter criterion for perturbativity, such as $\lambda_i < 4\pi$ or $\lambda_i < 1$, affects the allowed region in the parameter space only mildly. This stems from the fact that an $\mathcal{O}(1)$ coupling becomes nonperturbative very quickly.

JHEP05(2015)057

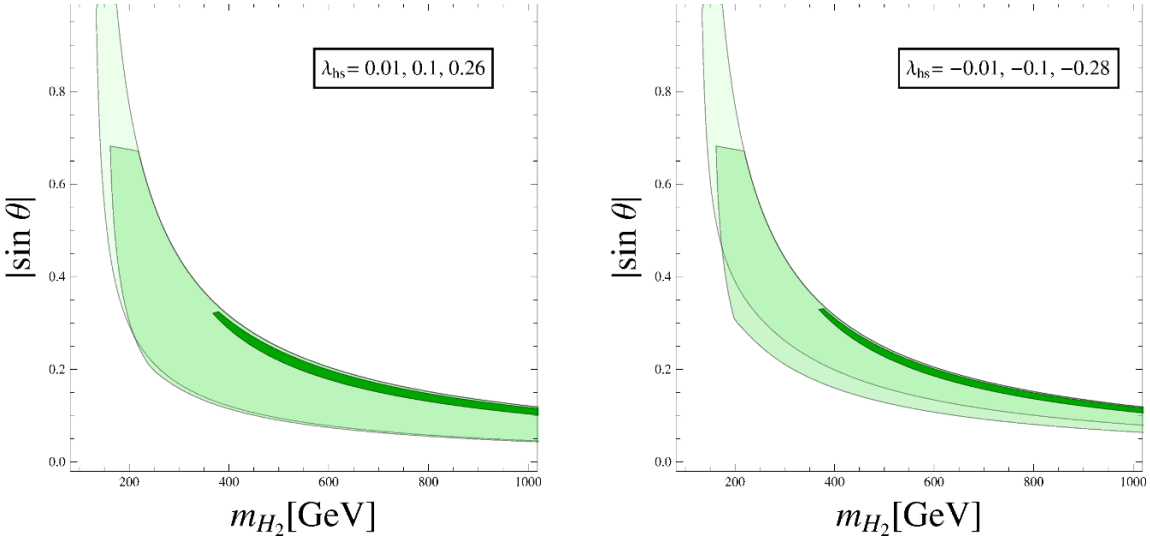

Figure 1. *Left:* Regions of parameter space (shaded) where the couplings remain perturbative and the electroweak vacuum remains stable up to the Planck scale, for $\lambda_{hs} = 0.01$ at the electroweak scale (lightest green), $\lambda_{hs} = 0.1$ (green), $\lambda_{hs} = 0.26$ (darkest green). *Right:* Analogous plot for negative values of λ_{hs}, namely $\lambda_{hs} = -0.01$ (lightest green), $\lambda_{hs} = -0.1$ (green), $\lambda_{hs} = -0.28$ (darkest green).

- At the upper boundary of each of the allowed regions the coupling λ_h becomes non-perturbative below m_P. Note that the initial value for λ_h at the weak scale grows with $|\sin\theta|$ as well as with m_{H_2}. Since the beta function of λ_h has a positive contribution proportional to λ_h^2, it is clear that above a certain curve (which roughly has the shape $|\sin\theta| \propto 1/m_{H_2}$), the initial values are so large that λ_h does not remain perturbative up to m_P.

- The limiting factor that determines the lower edge of the allowed regions depends on the value of λ_{hs}:

  - For small λ_{hs} ($\lambda_{hs} = \pm 0.01$), the lower edge is determined by stability of the potential. Since the initial value of λ_h decreases with decreasing $|\sin\theta|$ as well as with m_{H_2}, below a certain curve (which again roughly has the shape $|\sin\theta| \propto 1/m_{H_2}$), the additional threshold contribution $\lambda_h - \lambda_h^{SM}$ becomes too small to either keep $\lambda_h > 0$ (for $\lambda_{hs} > 0$) or satisfy $\lambda_h > \lambda_{hs}^2/(4\lambda_s)$ (for $\lambda_{hs} < 0$) all the way up to m_P.

  - For sizeable λ_{hs} ($\lambda_{hs} = 0.26$ and $\lambda_{hs} = -0.28$), perturbativity of λ_s is more constraining than stability of the vacuum, i.e. at the lower edge of the allowed regions the coupling λ_s becomes non-perturbative below m_P. Since, for substantial m_{H_2} and small $\sin\theta$, $\lambda_s \propto 1/\sin^2\theta \times 1/m_{H_2}^2$, the lower edge has the shape $|\sin\theta| \propto 1/m_{H_2}$.

    The reason why perturbativity becomes more constraining lies in the positive contribution $\propto \lambda_{hs}^2$ to the beta-functions of λ_s and λ_{hs}. Increasing $|\lambda_{hs}|$ shrinks

JHEP05(2015)057

the allowed region further, eventually leaving no allowed parameter space.

– For intermediate values of λ_{hs} ($\lambda_{hs} = \pm 0.1$), the limiting factor at the upper left side of the lower edge is perturbativity of λ_s, while vacuum stability is the limiting factor for the rest of the lower edge. The transition between the two is at the (hardly visible) kink of the lower edge of the plots.

Finally, let us note that if H_2 is lighter than the SM-like state H_1, the quartic coupling λ_h at the electroweak scale is *smaller* than that in the SM, which makes it harder to achieve stability of the electroweak vacuum. On the other hand, the one-loop correction due to λ_{hs} is positive and, if sufficiently large, could overcome the above tree-level setback. We find that this is possible if $4\lambda_h\lambda_s - \lambda_{hs}^2$ is positive yet very close to zero at m_t, with roughly $\lambda_{hs} \sim 0.3165$, $m_{H_2} \lesssim 0.6\,\text{GeV}$ and $\sin\theta \lesssim 0.04$. However, we find that $4\lambda_h\lambda_s - \lambda_{hs}^2$ runs negative already tens of GeV above m_t, which shows that to establish the existence of this minimum in the scalar potential would require a more sophisticated analysis of the full Coleman-Weinberg potential including the 2-loop effects. Since this region of parameter space is excluded experimentally due to the efficient $H_1 \to H_2 H_2$ decay (cf. section 4.2), we do not study it in more detail.

4 Experimental constraints

In this section we discuss the experimental constraints on a singlet scalar mixing with the Higgs boson.

4.1 Limits from electroweak precision data

In our model, electroweak observables are affected at leading order only via oblique corrections, that is via one-loop contributions to the propagators of the W and Z bosons. These corrections come from two sources: i) loop diagrams with the new scalar H_2, and ii) modified couplings of the 125 GeV scalar H_1 to the gauge bosons.

We define the propagator function Π_{VV} via the 2-point amplitude $\mathcal{M}(V_\mu \to V_\nu) = \eta_{\mu\nu}\Pi_{VV}(p^2) + \ldots$. In dimensional regularisation, the shift of the propagator function with respect to the SM is given by

$$\delta\Pi_{VV}(p^2) = \frac{m_V^2 \sin^2\theta}{4\pi^2 v^2}\left[\frac{m_{H_2}^2 - m_{H_1}^2}{4}\left(\frac{1}{\epsilon}+1\right) + F(p^2, m_V^2, m_{H_2}^2) - F(p^2, m_V^2, m_{H_1}^2)\right], \tag{4.1}$$

where $V = W, Z$ and the loop function F is defined by

$$F(p^2, m_V^2, m_\phi^2) = \int_0^1 dx \left[m_V^2 - \frac{\Delta}{2}\right]\log\Delta, \quad \text{with} \quad \Delta = x m_\phi^2 + (1-x)m_V^2 - p^2 x(1-x)\,. \tag{4.2}$$

The $1/\epsilon$ divergence cancels in physical observables.

The observables used in our fit are the LEP-1 Z-pole observables [28], the W mass [29], the total width [30], and the hadronic width [31], see table 1. The W and Z partial decay widths appearing in the table are given by

$$\Gamma(Z \to f\bar{f}) = \frac{N_f m_Z}{24\pi} g_{fZ;\text{eff}}^2, \qquad \Gamma(W \to f f') = \frac{N_f m_W}{48\pi} g_{fW;\text{eff}}^2 \tag{4.3}$$

JHEP05(2015)057

observable	experimental value	ref.	SM prediction	definition
Γ_Z [GeV]	2.4952 ± 0.0023	[28]	2.4950	$\sum_f \Gamma(Z \to f\bar{f})$
$\sigma_{\rm had}$ [nb]	41.540 ± 0.037	[28]	41.484	$\frac{12\pi}{m_Z^2}\frac{\Gamma(Z\to e^+e^-)\Gamma(Z\to q\bar{q})}{\Gamma_Z^2}$
R_ℓ	20.767 ± 0.025	[28]	20.743	$\frac{\sum_q \Gamma(Z\to q\bar{q})}{\Gamma(Z\to \ell^+\ell^-)}$
A_ℓ	0.1499 ± 0.0018	[32]	0.1472	$\frac{\Gamma(Z\to e_L^+e_L^-)-\Gamma(Z\to e_R^+e_R^-)}{\Gamma(Z\to e^+e^-)}$
$A_{\rm FB}^{0,\ell}$	0.0171 ± 0.0010	[28]	0.0163	$\frac{3}{4}A_\ell^2$
$\sin^2\theta_{\rm eff}^\ell(Q_{\rm FB})$	0.2324 ± 0.0012	[28]	0.23150	$\frac{g_Y^2}{g_L^2+g_Y^2}(1-\frac{g_L\delta\Pi_{Z\gamma}(m_Z^2)}{g_Y m_Z^2})$
R_b	0.21629 ± 0.00066	[28]	0.21578	$\frac{\Gamma(Z\to d\bar{d})}{\sum_q \Gamma(Z\to q\bar{q})}$
A_b	0.923 ± 0.020	[28]	0.935	$\frac{\Gamma(Z\to d_L\bar{d}_L)-\Gamma(Z\to d_R\bar{d}_R)}{\Gamma(Z\to d\bar{d})}$
$A_b^{\rm FB}$	0.0992 ± 0.0016	[28]	0.1032	$\frac{3}{4}A_\ell A_b$
R_c	0.1721 ± 0.0030	[28]	0.17226	$\frac{\Gamma(Z\to u\bar{u})}{\sum_q \Gamma(Z\to q\bar{q})}$
A_c	0.670 ± 0.027	[28]	0.668	$\frac{\Gamma(Z\to u_L\bar{u}_L)-\Gamma(Z\to u_R\bar{u}_R)}{\Gamma(Z\to u\bar{u})}$
$A_c^{\rm FB}$	0.0707 ± 0.0035	[28]	0.0738	$\frac{3}{4}A_\ell A_c$
m_W [GeV]	80.385 ± 0.015	[29]	80.3602	$\sqrt{\frac{g_L^2v^2}{4}+\delta\Pi_{WW}(m_W^2)}$
Γ_W [GeV]	2.085 ± 0.042	[30]	2.091	$\sum_f \Gamma(W\to f f')$
Br($W \to$ had)	0.6741 ± 0.0027	[31]	0.6751	$\frac{\sum_q \Gamma(W\to q q')}{\sum_f \Gamma(W\to f f')}$

Table 1. The electroweak precision observables used in this analysis. We take into account the experimental correlations between the LEP-1 Z-pole observables and between the heavy flavour observables. For the theoretical predictions we use the best fit SM values from GFitter [32], except for Br($W \to$ had) where we take the value quoted in [31].

where N_f is the number of colours of the fermion f and the effective couplings are defined as (see e.g. [33])

$$g_{fZ;\rm eff} = \frac{\sqrt{g_L^2+g_Y^2}}{\sqrt{1-\delta\Pi'_{ZZ}(m_Z^2)}}\left[T_f^3 - Q_f s^2_{\rm eff}\right], \quad s^2_{\rm eff} = \frac{g_Y^2}{g_L^2+g_Y^2}\left(1-\frac{g_L}{g_Y}\frac{\delta\Pi_{\gamma Z}(m_Z^2)}{m_Z^2}\right),$$
$$g_{fW;\rm eff} = g_{W;\rm eff} = \frac{g_L}{\sqrt{1-\delta\Pi'_{WW}(m_W^2)}}, \tag{4.4}$$

where g_L and g_Y are the gauge couplings of SU(2) × U(1). Note that in our model $\delta\Pi_{\gamma Z}$ as well as $\delta\Pi_{\gamma\gamma}$ vanish at one-loop level. As is customary, the SM electroweak parameters g_L, g_Y, v are taken from the input observables G_F, α and m_Z. The oblique corrections also contribute to our input observables, effectively shifting the electroweak parameters by

$$\frac{\delta g_L}{g_L} = \frac{1}{g_L^2-g_Y^2}\left(2\frac{\delta\Pi_{WW}(0)}{v^2} - 2\cos^2\theta_W\frac{\delta\Pi_{ZZ}(m_Z^2)}{v^2} + \frac{g_Y^2}{2}\delta\Pi'_{\gamma\gamma}(0)\right),$$
$$\frac{\delta g_Y}{g_Y} = \frac{1}{g_L^2-g_Y^2}\left(-\frac{2g_Y^2}{g_L^2}\frac{\delta\Pi_{WW}(0)}{v^2} + 2\sin^2\theta_W\frac{\delta\Pi_{ZZ}(m_Z^2)}{v^2} - \frac{g_L^2}{2}\delta\Pi'_{\gamma\gamma}(0)\right),$$
$$\frac{\delta v}{v} = -\frac{2\delta\Pi_{WW}(0)}{g_L^2v^2}. \tag{4.5}$$

Using eqs. (4.4) and (4.5) one can calculate how the effective couplings (and hence, by eq. (4.3), the partial decay widths) are shifted in the presence of oblique corrections, and

JHEP05(2015)057

Channel	μ (ATLAS)	μ (CMS)
$H_1 \to \gamma\gamma$	$1.17^{+0.27}_{-0.27}$ [34]	$1.12^{+0.24}_{-0.24}$ [38]
$H_1 \to ZZ^* \to 4\ell$	$1.44^{+0.40}_{-0.33}$ [37]	$1.00^{+0.29}_{-0.29}$ [38]

Table 2. The signal strength of the 125 GeV scalar relative to that of the SM Higgs measured at the LHC in the $\gamma\gamma$ and 4ℓ channels.

compute the corrections to precision observables. We take into account the leading order (linear) corrections in $\delta\Pi_{VV}$. Using the observables in table 1, we construct a global χ^2 function that depends on m_{H_2}, $\sin\theta$, and known SM parameters. For each m_{H_2} we minimise the global χ^2 with respect to $\sin\theta$, and determine the 95% CL limits by solving

$$\chi^2(m_{H_2}, \sin\theta) - \min_\theta\{\chi^2(m_{H_2}, \sin\theta)\} = 3.84\,. \tag{4.6}$$

The excluded region is shown as the grey area in figure 3. The limits are non-trivial for $m_{H_2} \lesssim 60\,\text{GeV}$ and $m_{H_2} \gtrsim 170\,\text{GeV}$, and become stronger as H_2 gets heavier. For $m_{H_2} \gtrsim 450\,\text{GeV}$, the electroweak precision constraints provide the strongest limits on the model.[3]

4.2 Limits from Higgs coupling measurements

An important constraint on the model comes from the fact that mixing with the singlet modifies the coupling strength of the Higgs boson to the SM gauge bosons and fermions. The couplings of the 125 GeV boson, here identified with H_1, have recently been measured at the LHC in several decay channels. Here we only use the results with the $\gamma\gamma$ and 4ℓ final states that have the best mass resolution. This allows us to simplify the discussion of possible contamination of the H_1 signal strength measurements by H_2 decays. We will assume that for m_{H_2} outside the interval $[120, 130]\,\text{GeV}$ this contamination is absent, as suggested by the results of ATLAS and CMS Higgs searches in these two channels. In order to determine the limits on $\sin\theta$ for $m_{H_2} \in [120, 130]\,\text{GeV}$, one needs a more elaborate analysis that takes into account a different mass resolution in various $h \to \gamma\gamma$ and $h \to 4\ell$ search categories. We will not attempt such an analysis in this paper.

We use the most recent inclusive H_1 signal strengths measurements by ATLAS and CMS collected in table 2. Moreover, we take into account the 15% theoretical uncertainty in the Higgs production cross section, which is a linear sum of the PDF and QCD scale errors on the gluon fusion cross section [39]. We include this uncertainty as a Gaussian-modeled nuisance parameter. With this procedure, we get the combined constraint on the

[3]Using eq. (4.1) one could also compute the usual Peskin-Takeuchi S and T parameters, which in the case at hand are $S = \frac{16\pi\cos^2\theta_W}{g^2}\delta\Pi'_{ZZ}(0)$, $T = \frac{4\pi}{e^2}\left(\frac{\delta\Pi_{WW}(0)}{m_W^2} - \frac{\delta\Pi_{ZZ}(0)}{m_Z^2}\right)$. For $m_{H_2} \gg m_{H_1}$ this gives

$$T \approx -\frac{3}{8\pi\cos^2\theta_W}\sin^2\theta\log(m_{H_2}/M_T), \qquad S \approx \frac{1}{6\pi}\sin^2\theta\log(m_{H_2}/M_S),$$

where $M_T \approx 211\,\text{GeV}$, $M_S \approx 81\,\text{GeV}$. The resulting constraints from S and T indeed give a good approximation (within 10%) of the actual limits for $m_{H_2} \gtrsim 400\,\text{GeV}$. We stress that our analysis is valid for any m_{H_2}, in particular also for $m_{H_2} \ll m_{H_1}$.

JHEP05(2015)057

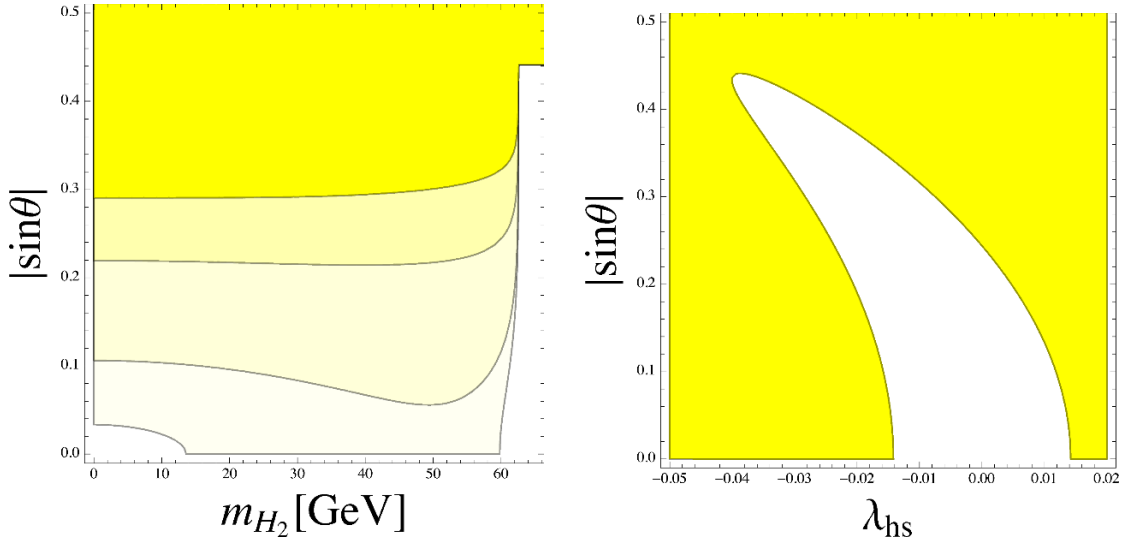

Figure 2. *Left:* Regions of parameter space for $m_{H_2} < 65\,\text{GeV}$ excluded at 95% CL by the limits on the H_1 coupling. The excluded areas (in yellow) correspond to $\lambda_{hs} = -0.011, 0.0001, 0.011, 0.014$ (from the darkest to the palest). *Right:* The excluded region (in yellow) for $m_{H_2} = 20\,\text{GeV}$. Inside the white region the $H_1 H_2^2$ coupling is very small.

Higgs signal strength

$$\mu > 0.81, \qquad @95\%\ \text{CL}. \tag{4.7}$$

For $m_{H_2} \geq m_{H_1}/2 \sim 62.5\,\text{GeV}$ and m_{H_2} outside the [120,130] GeV interval, this translates to a bound on $\sin\theta$,

$$\sin\theta < 0.44, \qquad @95\%\ \text{CL}, \tag{4.8}$$

that is independent of m_{H_2}.

For $m_{H_2} < m_{H_1}/2$ the situation is more complicated because the $H_1 \to H_2 H_2$ decay channel opens up, leading to a decrease of the signal strength in all visible channels. This typically leads to stronger limits on $\sin\theta$, which are slightly dependent on m_{H_2} and strongly on λ_{hs}. Representative examples of these constraints are shown in figure 2. A larger $|\lambda_{hs}|$ normally entails stronger limits and at some point almost the entire m_{H_2}–$\sin\theta$ plane gets excluded. Thus, at low m_{H_2}, the allowed λ_{hs} is typically limited to the range $|\lambda_{hs}| < 0.015$. Nevertheless, for a given m_{H_2} and $\sin\theta$ one can always adjust a negative λ_{hs} such that the $H_1 H_2^2$ coupling vanishes, in which case the limit is that of eq. (4.8). The region excluded by H_1 coupling measurements is marked as the yellow area in figure 3.

4.3 Limits from direct searches for a Higgs-like scalar

Further constraints are provided by the LEP and LHC searches for a Higgs-like scalar. We take into account the following results:

- Searches for $H_2 \to \gamma\gamma$ in ATLAS [35] and CMS [36].
- Searches for $H_2 \to ZZ$ in the 4ℓ channel in ATLAS [37] and CMS [40].

JHEP05(2015)057

- Searches for $H_2 \to WW$ in the $e\mu 2\nu$ channel in ATLAS [41].
- $H_2 \to H_1 H_1$ searches in CMS with the $2b\,2\gamma$ [42] and $4b$ [43] final states, and in ATLAS with the $2b\,2\gamma$ final state [44].
- LEP Higgs searches [45] dominated by the $b\bar{b}$ decay channel.
- DELPHI search for a low mass Higgs in Z-decays [46].
- b-physics constraints on a low mass Higgs [47–49].

The parameter space excluded by these searches is shown as the red area in figure 3. At very low masses, $m_{H_2} < 5\,\text{GeV}$, the strongest limits come from $B \to K\ell\ell$ decays [47, 48]. The resulting constraint $\sin\theta < 10^{-2} \ldots 10^{-3}$ can be extracted from the analysis of ref. [50]. Between 5 GeV and 12 GeV, the bound $\sin\theta \lesssim 0.5$ is imposed by the radiative Υ decays [49] and the DELPHI searches for a light Higgs in Z-decays [46]. Above this mass window up to about 115 GeV, LEP Higgs searches [45] become relevant. The resulting bound on $\sin\theta$ is about 1×10^{-1} to few$\times 10^{-1}$ depending on the exact H_2 mass. The region between 120 and 130 GeV remains poorly constrained due to the presence of the SM-like Higgs,[4] whereas a strip just below and above it is constrained through the diphoton channel searches [35, 36] although the bound is still looser than the indirect one from the H_1 coupling measurements. Above 130 GeV the limits are dominated by the 4ℓ channel [37, 40]. This imposes $\sin\theta < 0.3 \ldots 0.4$ in a wide range of masses up to about 450 GeV, above which the indirect bounds are consistently stronger.

Concerning the λ_{hs}-dependence of the exclusion limits, let us note that the limits on $(m_{H_2}, \sin\theta)$ can be much stronger for a given λ_{hs}. In particular, for $2m_{H_2} \leq m_{H_1}$ the $H_1 \to H_2 H_2$ decay would dilute the Higgs signal strength as explained in the previous subsection. Therefore, in figure 3 we marginalise over λ_{hs} in this mass region. For $m_{H_2} > 2m_{H_1}$ the limits also depend on λ_{hs}: the larger it is, the more suppressed is the $H_2 \to 4\ell$ channel, and the more enhanced is the $H_2 \to H_1 H_1$ decay. However, this effect is non-negligible only for $\lambda_{hs} \gtrsim 1$; for smaller values the limits depend very little on the precise value of λ_{hs}. The constraints from $H_2 \to H_1 H_1$ are more important than those from $H_2 \to 4\ell$ only for $\lambda_{hs} \gtrsim 2$; for no perturbative value of λ_{hs} are these limits stronger than the indirect ones from the H_1 coupling measurements.

4.4 Combined experimental constraints vs. vacuum stability

Combining the bounds from direct searches, precision tests, and H_1 coupling measurements and imposing them on the parameter space favoured by the stability considerations in figure 3 (green), we find that for $m_{H_2} \gtrsim 160\,\text{GeV}$ all of the constraints are compatible. Almost the entire stability-favoured region above 300 GeV is unconstrained, whereas between 160 and 300 GeV there are pockets of allowed parameter space with $\sin\theta$ between 0.2 and 0.4.

The favoured region can be probed further by measuring the Higgs signal strength with higher precision as well as by searching for the decay $H_2 \to H_1 H_1$.

[4] This allows for an almost degenerate second Higgs with a large mixing between the two [51].

JHEP05(2015)057

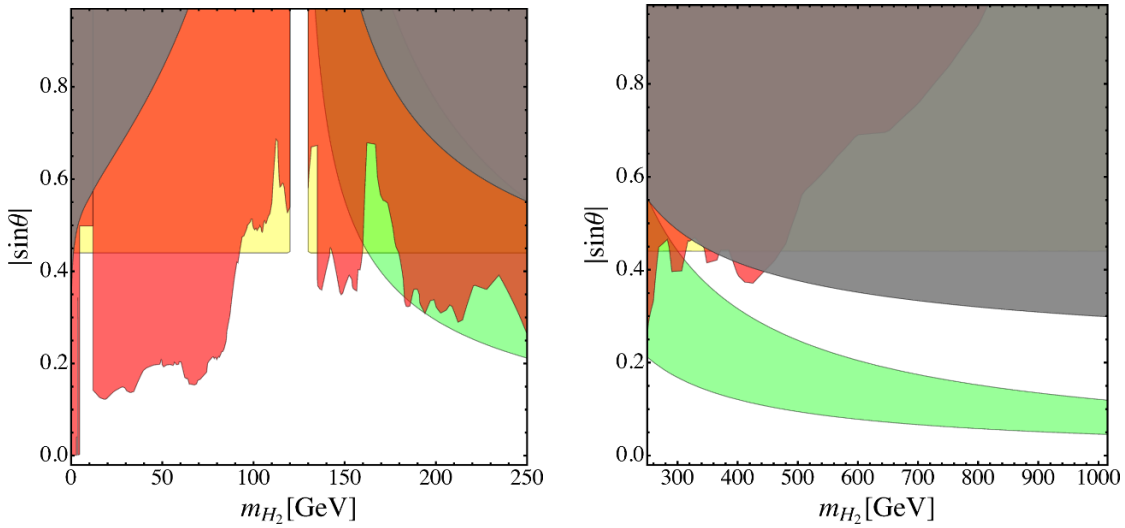

Figure 3. *Left:* Parameter space (for $m_{H_2} \leq 2m_{H_1}$) excluded at 95 % CL by direct searches (red), precision tests (gray), and H_1 couplings measurements (yellow). For $m_{H_2} < m_{H_1}/2$, the limit from the H_1 couplings is marginalised over λ_{hs}, otherwise it does not depend on λ_{hs}. The green region is preferred by stability of the scalar potential up to the Planck scale at $\lambda_{hs} = 0.01$; for other λ_{hs}, it is either very similar or smaller and contained within the green region. *Right:* Same for $m_{H_2} > 2m_{H_1}$.

5 Prospects for observing $H_2 \to H_1H_1$ at LHC-13

For $m_{H_2} > 250\,\text{GeV}$, the decay $H_2 \to H_1H_1$ is allowed kinematically. It is an important channel for studying properties of H_2, which allows for a reconstruction of λ_{hs} [21, 22]. The rate of $H_2 \to H_1H_1$ depends on $\sin\theta$, m_{H_2} and also λ_{hs}, cf. eq. (2.14a). While the first two parameters can be fixed using the SM-like decay modes of H_2, determination of λ_{hs} requires an additional channel such as $H_2 \to H_1H_1$.

The left panel of figure 4 displays contours of equal $\sigma(pp \to H_2)\,\text{BR}(H_2 \to H_1H_1)$ in the $\sin\theta - m_{H_2}$ plane, while the right panel shows the maximal production rate $\sigma(pp \to H_2)\,\text{BR}(H_2 \to H_1H_1)$ at LHC-13 consistent with all the experimental constraints. The different curves in the right panel correspond to different λ_{hs}. At fixed λ_{hs}, the rate is restricted by the bound on $\sin\theta$ which is mostly due to the LHC constraints for $m_{H_2} < 450\,\text{GeV}$ and to the electroweak constraints for $m_{H_2} > 450\,\text{GeV}$. The rate also increases with λ_{hs}, which we take to be $0.01, 1, 2$ in the plot. In all of these cases, $\sigma(pp \to H_2)\,\text{BR}(H_2 \to H_1H_1)$ is in the picobarn range for m_{H_2} up to about 400 GeV. This makes the prospects for detecting $H_2 \to H_1H_1$ at LHC-13 quite good, at least for a relatively light H_2.

Imposing the extra stability/perturbativity constraint up to m_P, we find reduction of the maximal rate for m_{H_2} above around 350 GeV. This theoretical constraint becomes the strongest bound on the model, with the preferred parameter space being difficult to probe experimentally. For light H_2 however, the main constraints are due to the LHC heavy Higgs searches which allow for a substantial rate $\sigma(pp \to H_2)\,\text{BR}(H_2 \to H_1H_1)$.

JHEP05(2015)057

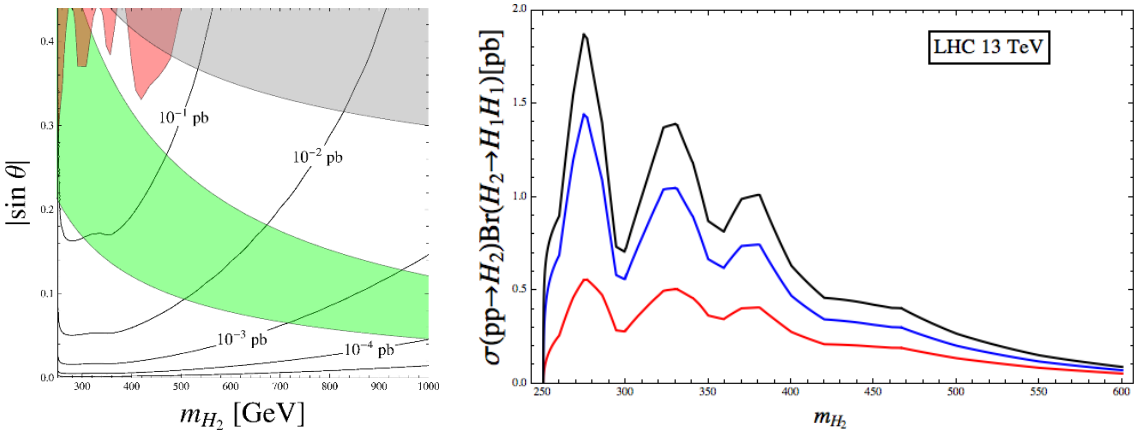

Figure 4. *Left:* $\sigma(pp \to H_2)$ BR$(H_2 \to H_1 H_1)$ at LHC-13 for $\lambda_{hs} = 0.01$ in the $\sin\theta$-m_{H_2} plane. *Right:* $\sigma(pp \to H_2)$ BR$(H_2 \to H_1 H_1)$ at LHC-13 for maximal allowed values of $\sin\theta$, with $\lambda_{hs} = 0.01$ (bottom), $\lambda_{hs} = 1$ (middle), $\lambda_{hs} = 2$ (top). m_{H_2} is in GeV.

6 Summary and conclusions

We have analysed constraints on the two scalar states of the simplest Higgs portal model. One of them is identified with the 125 GeV Higgs-like boson observed at the LHC. The other boson's mass is allowed to be in a wide range down to about 5 GeV, below which the constraints on the mixing angle become severe. Above ~ 90 GeV, a substantial mixing between the Higgs and the singlet, $\sin\theta \sim 0.3 \ldots 0.4$, is consistent with the data.

Stability of the scalar potential can be improved over that of the SM if the state H_2 is sufficiently heavy, above about 160 GeV. For a range of $\sin\theta$ consistent with the electroweak precision measurements and the LHC data, the electroweak vacuum is stable and the model is perturbative up to the Planck scale. The required mixing angle is of order 10^{-1} for m_{H_2} up to 1 TeV.

In the allowed parameter space, the decay $H_2 \to H_1 H_1$ can be quite efficient such that the H_1 pair production rate at LHC-13 is at the picobarn level. This applies to a relatively light H_2 up to about 400 GeV, with the rate quickly falling off above 500 GeV or so. Apart from the search for a new resonance, the Higgs portal can be efficiently constrained by further improvement of the Higgs coupling measurements.

Acknowledgments

This work was supported in part by the Academy of Finland project "The Higgs boson and the Cosmos". AF is supported by the ERC Advanced Grant Higgs@LHC.

N.B. At the time of completion of this work, we became aware of the preprints arXiv:1501.02234 (ref. [15–17]) and arXiv:1501.03799 (ref. [20]) which have some overlap with our study.

JHEP05(2015)057

References

[1] V. Silveira and A. Zee, *SCALAR PHANTOMS*, *Phys. Lett.* **B 161** (1985) 136 [INSPIRE].

[2] R. Schabinger and J.D. Wells, *A Minimal spontaneously broken hidden sector and its impact on Higgs boson physics at the large hadron collider*, *Phys. Rev.* **D 72** (2005) 093007 [hep-ph/0509209] [INSPIRE].

[3] B. Patt and F. Wilczek, *Higgs-field portal into hidden sectors*, hep-ph/0605188 [INSPIRE].

[4] D. O'Connell, M.J. Ramsey-Musolf and M.B. Wise, *Minimal Extension of the Standard Model Scalar Sector*, *Phys. Rev.* **D 75** (2007) 037701 [hep-ph/0611014] [INSPIRE].

[5] V. Barger, P. Langacker, M. McCaskey, M.J. Ramsey-Musolf and G. Shaughnessy, *LHC Phenomenology of an Extended Standard Model with a Real Scalar Singlet*, *Phys. Rev.* **D 77** (2008) 035005 [arXiv:0706.4311] [INSPIRE].

[6] D. Bertolini and M. McCullough, *The Social Higgs*, *JHEP* **12** (2012) 118 [arXiv:1207.4209] [INSPIRE].

[7] C. Englert, J. Jaeckel, V.V. Khoze and M. Spannowsky, *Emergence of the Electroweak Scale through the Higgs Portal*, *JHEP* **04** (2013) 060 [arXiv:1301.4224] [INSPIRE].

[8] E. Gabrielli et al., *Towards Completing the Standard Model: Vacuum Stability, EWSB and Dark Matter*, *Phys. Rev.* **D 89** (2014) 015017 [arXiv:1309.6632] [INSPIRE].

[9] D. Buttazzo et al., *Investigating the near-criticality of the Higgs boson*, *JHEP* **12** (2013) 089 [arXiv:1307.3536] [INSPIRE].

[10] F. Bezrukov, M.Y. Kalmykov, B.A. Kniehl and M. Shaposhnikov, *Higgs Boson Mass and New Physics*, *JHEP* **10** (2012) 140 [arXiv:1205.2893] [INSPIRE].

[11] S. Alekhin, A. Djouadi and S. Moch, *The top quark and Higgs boson masses and the stability of the electroweak vacuum*, *Phys. Lett.* **B 716** (2012) 214 [arXiv:1207.0980] [INSPIRE].

[12] O. Lebedev and A. Westphal, *Metastable Electroweak Vacuum: Implications for Inflation*, *Phys. Lett.* **B 719** (2013) 415 [arXiv:1210.6987] [INSPIRE].

[13] O. Lebedev, *On Stability of the Electroweak Vacuum and the Higgs Portal*, *Eur. Phys. J.* **C 72** (2012) 2058 [arXiv:1203.0156] [INSPIRE].

[14] J. Elias-Miro, J.R. Espinosa, G.F. Giudice, H.M. Lee and A. Strumia, *Stabilization of the Electroweak Vacuum by a Scalar Threshold Effect*, *JHEP* **06** (2012) 031 [arXiv:1203.0237] [INSPIRE].

[15] G.M. Pruna and T. Robens, *Higgs singlet extension parameter space in the light of the LHC discovery*, *Phys. Rev.* **D 88** (2013) 115012 [arXiv:1303.1150] [INSPIRE].

[16] D. Lopez-Val and T. Robens, *Δr and the W-boson mass in the singlet extension of the standard model*, *Phys. Rev.* **D 90** (2014) 114018 [arXiv:1406.1043] [INSPIRE].

[17] T. Robens and T. Stefaniak, *Status of the Higgs Singlet Extension of the Standard Model after LHC Run 1*, *Eur. Phys. J.* **C 75** (2015) 104 [arXiv:1501.02234] [INSPIRE].

JHEP05(2015)057

[18] S. Profumo, M.J. Ramsey-Musolf, C.L. Wainwright and P. Winslow, *Singlet-catalyzed electroweak phase transitions and precision Higgs boson studies*, *Phys. Rev.* **D 91** (2015) 035018 [arXiv:1407.5342] [INSPIRE].

[19] C.-Y. Chen, S. Dawson and I.M. Lewis, *Exploring resonant di-Higgs boson production in the Higgs singlet model*, *Phys. Rev.* **D 91** (2015) 035015 [arXiv:1410.5488] [INSPIRE].

[20] V. Martin-Lozano, J.M. Moreno and C.B. Park, *Resonant Higgs boson pair production in the $hh \to b\bar{b}\,WW \to b\bar{b}\ell^+\nu\ell^-\bar{\nu}$ decay channel*, arXiv:1501.03799 [INSPIRE].

[21] C. Englert, T. Plehn, D. Zerwas and P.M. Zerwas, *Exploring the Higgs portal*, *Phys. Lett.* **B 703** (2011) 298 [arXiv:1106.3097] [INSPIRE].

[22] C. Englert, M. Spannowsky and C. Wymant, *Partially (in)visible Higgs decays at the LHC*, *Phys. Lett.* **B 718** (2012) 538 [arXiv:1209.0494] [INSPIRE].

[23] J.M. No and M. Ramsey-Musolf, *Probing the Higgs Portal at the LHC Through Resonant di-Higgs Production*, *Phys. Rev.* **D 89** (2014) 095031 [arXiv:1310.6035] [INSPIRE].

[24] O. Lebedev and H.M. Lee, *Higgs Portal Inflation*, *Eur. Phys. J.* **C 71** (2011) 1821 [arXiv:1105.2284] [INSPIRE].

[25] M. Gonderinger, H. Lim and M.J. Ramsey-Musolf, *Complex Scalar Singlet Dark Matter: Vacuum Stability and Phenomenology*, *Phys. Rev.* **D 86** (2012) 043511 [arXiv:1202.1316] [INSPIRE].

[26] V.V. Khoze, C. McCabe and G. Ro, *Higgs vacuum stability from the dark matter portal*, *JHEP* **08** (2014) 026 [arXiv:1403.4953] [INSPIRE].

[27] S. Moch, *Precision determination of the top-quark mass*, PoS(LL2014)054 [arXiv:1408.6080] [INSPIRE].

[28] ALEPH, DELPHI, L3, OPAL, SLD, LEP Electroweak Working Group, SLD Electroweak Group, SLD Heavy Flavour Group collaboration, S. Schael et al., *Precision electroweak measurements on the Z resonance*, *Phys. Rept.* **427** (2006) 257 [hep-ex/0509008] [INSPIRE].

[29] CDF, D0 collaboration, T.E.W. Group, *2012 Update of the Combination of CDF and D0 Results for the Mass of the W Boson*, arXiv:1204.0042 [INSPIRE].

[30] Particle Data Group collaboration, J. Beringer et al., *Review of Particle Physics (RPP)*, *Phys. Rev.* **D 86** (2012) 010001 [INSPIRE].

[31] ALEPH, DELPHI, L3, OPAL, LEP Electroweak collaboration, S. Schael et al., *Electroweak Measurements in Electron-Positron Collisions at W-Boson-Pair Energies at LEP*, *Phys. Rept.* **532** (2013) 119 [arXiv:1302.3415] [INSPIRE].

[32] Gfitter Group collaboration, M. Baak et al., *The global electroweak fit at NNLO and prospects for the LHC and ILC*, *Eur. Phys. J.* **C 74** (2014) 3046 [arXiv:1407.3792] [INSPIRE].

[33] J.D. Wells, *TASI lecture notes: Introduction to precision electroweak analysis*, hep-ph/0512342 [INSPIRE].

[34] ATLAS collaboration, *Measurement of Higgs boson production in the diphoton decay channel in pp collisions at center-of-mass energies of 7 and 8 TeV with the ATLAS detector*, *Phys. Rev.* **D 90** (2014) 112015 [arXiv:1408.7084] [INSPIRE].

[35] ATLAS collaboration, *Search for Scalar Diphoton Resonances in the Mass Range $65 - 600$ GeV with the ATLAS Detector in pp Collision Data at $\sqrt{s} = 8$ TeV*, *Phys. Rev. Lett.* **113** (2014) 171801 [arXiv:1407.6583] [INSPIRE].

JHEP05(2015)057

[36] CMS collaboration, *Observation of the diphoton decay of the Higgs boson and measurement of its properties*, *Eur. Phys. J.* **C 74** (2014) 3076 [arXiv:1407.0558] [INSPIRE].

[37] ATLAS collaboration, *Measurements of Higgs boson production and couplings in the four-lepton channel in pp collisions at center-of-mass energies of 7 and 8 TeV with the ATLAS detector*, *Phys. Rev.* **D 91** (2015) 012006 [arXiv:1408.5191] [INSPIRE].

[38] CMS collaboration, *Precise determination of the mass of the Higgs boson and tests of compatibility of its couplings with the standard model predictions using proton collisions at 7 and 8 TeV*, arXiv:1412.8662 [INSPIRE].

[39] LHC Higgs Cross Section Working Group collaboration, S. Dittmaier et al., *Handbook of LHC Higgs Cross Sections: 1. Inclusive Observables*, arXiv:1101.0593 [INSPIRE].

[40] CMS collaboration, *Measurement of the properties of a Higgs boson in the four-lepton final state*, *Phys. Rev.* **D 89** (2014) 092007 [arXiv:1312.5353] [INSPIRE].

[41] ATLAS collaboration, *Search for a high-mass Higgs boson in the $H \to WW \to l\nu l\nu$ decay channel with the ATLAS detector using 21 fb^{-1} of proton-proton collision data*, ATLAS-CONF-2013-067 (2013).

[42] CMS collaboration, *Search for resonant HH production in 2gamma+2b channel*, CMS-PAS-HIG-13-032 (Search for resonant HH production in 2gamma+2b channel).

[43] CMS collaboration, *Search for di-Higgs resonances decaying to 4 bottom quarks*, CMS-PAS-HIG-14-013 (Search for di-Higgs resonances decaying to 4 bottom quarks).

[44] ATLAS collaboration, *Search For Higgs Boson Pair Production in the $\gamma\gamma b\bar{b}$ Final State using pp Collision Data at $\sqrt{s} = 8$ TeV from the ATLAS Detector*, *Phys. Rev. Lett.* **114** (2015) 081802 [arXiv:1406.5053] [INSPIRE].

[45] LEP Working Group for Higgs boson searches, ALEPH, DELPHI, L3, OPAL collaboration, R. Barate et al., *Search for the standard model Higgs boson at LEP*, *Phys. Lett.* **B 565** (2003) 61 [hep-ex/0306033] [INSPIRE].

[46] DELPHI collaboration, P. Abreu et al., *Search for low mass Higgs bosons produced in Z0 decays*, *Z. Phys.* **C 51** (1991) 25 [INSPIRE].

[47] LHCb collaboration, *Differential branching fraction and angular analysis of the $B^+ \to K^+\mu^+\mu^-$ decay*, *JHEP* **02** (2013) 105 [arXiv:1209.4284] [INSPIRE].

[48] Belle collaboration, J.-T. Wei et al., *Measurement of the Differential Branching Fraction and Forward-Backword Asymmetry for $B \to K^*\ell^+\ell^-$*, *Phys. Rev. Lett.* **103** (2009) 171801 [arXiv:0904.0770] [INSPIRE].

[49] BaBar collaboration, J.P. Lees et al., *Search for di-muon decays of a low-mass Higgs boson in radiative decays of the $\Upsilon(1S)$*, *Phys. Rev.* **D 87** (2013) 031102 [arXiv:1210.0287] [INSPIRE].

[50] K. Schmidt-Hoberg, F. Staub and M.W. Winkler, *Constraints on light mediators: confronting dark matter searches with B physics*, *Phys. Lett.* **B 727** (2013) 506 [arXiv:1310.6752] [INSPIRE].

[51] M. Heikinheimo, A. Racioppi, M. Raidal and C. Spethmann, *Twin Peak Higgs*, *Phys. Lett.* **B 726** (2013) 781 [arXiv:1307.7146] [INSPIRE].

JHEP05(2015)057